Chemico-Biological Interactions 406 (2025) 111341

Contents lists available at ScienceDirect

Chemico-Biological Interactions

journal homepage: www.elsevier.com/locate/chembioint

Research paper

Deferoxamine-induced neurotoxicity: Role of chaperone-mediated autophagy dysfunction in neuronal apoptosis in the hippocampus

Hong Zhang [a], Jian Guo [a,b], Jiayi Chu [c], Huanhuan Yu [d], Jialin Zhang [a], Siman Ma [c], Ge Jin [e], Yingshan Jiang [c], Jiao Xiao [f], Yutong Hou [c], Minyan Li [d,**], Shiliang Yin [e,*]

[a] School of Life Science and Biopharmaceutics, Shenyang Pharmaceutical University, Shenyang, 110016, People's Republic of China
[b] Shenyang Kangende Medical Technology Co., Ltd, Shenyang, 110163, People's Republic of China
[c] School of Pharmacy, Shenyang Pharmaceutical University, Shenyang, 110016, People's Republic of China
[d] Department of Hematology, General Hospital of Northern Theater Command, Shenyang, 110016, People's Republic of China
[e] School of Pharmacy, Shenyang Medical College, Shenyang, 110034, People's Republic of China
[f] Wuya School of Innovation, Shenyang Pharmaceutical University, Shenyang, 110016, People's Republic of China

ARTICLE INFO

Keywords:
Deferoxamine mesylate
Neuronal adverse events
Chaperon mediated autophagy
Neuronal apoptosis

ABSTRACT

Deferoxamine mesylate (DFX) is a microorganism-derived iron chelator used in hematology to treat acute iron intoxication and chronic iron overload. Many studies have reported adverse neurological events from DFX exposure, but it is challenging to distinguish these from the effects of iron intoxication. This study aimed to evaluate whether DFX exposure alone can directly impair neurological functions and to elucidate its toxicological mechanisms. Our findings from *in vivo* and *in vitro* experiments indicate that DFX exposure can directly cause emotional and cognitive dysfunction in mice. Neuronal apoptosis, resulting from chaperone-mediated autophagy (CMS) dysfunction, was identified as a key toxicological mechanism underlying DFX-induced neuronal impairment. This study provides evidence for the comprehensive monitoring and timely management of neurotoxic adverse events associated with DFX exposure, as well as a foundation for developing medications to prevent and treat these events to enhance patient quality of life.

1. Introduction

Deferoxamine mesylate (DFX) is a natural product of soil bacteria such as *Streptomyces pilosus* and other actinomycetes [1]. DFX, as an iron chelator, is widely used in clinical hematology to treat acute iron intoxication and chronic iron overload caused by transfusion-dependent anemias [2]. Additionally, DFX has demonstrated efficacy in mitigating complications of sickle cell anemia and in prolonging the lifespan in patients with β-thalassemia to levels comparable to the general population [3,4].

Despite its significant therapeutic benefits in reducing the incidence and mortality linked to siderosis, clinical reports have documented a range of adverse events associated with DFX administration. In addition to localized injection site reactions, patients have exhibited growth retardation, endocrine dysfunction, and toxicity affecting the cardiovascular, pulmonary, kidney, and nervous systems [5–9]. Neurotoxicity is one of the most commonly reported adverse effects, manifesting as optic neuropathy, ototoxicity, and olfactory dysfunction, as well as more severe neurological disturbances, including dizziness, convulsions, and coma. These neurotoxic effects seriously limit the quality of life and pose life-threatening risks [2,10–16]. Notably, the clinical presentations of DFX-related neurotoxicity closely resemble those of iron poisoning, complicating differential diagnosis [17]. Additionally, some studies suggest that chronic aluminum exposure from DFX treatment may indirectly cause optical, auditory, and olfactory toxicities (Ellenberg et al., 1990; [18]). The question of whether DFX exposure can independently induce neurological impairments along with the underlying toxicological mechanisms remains unresolved, warranting further comprehensive investigations.

Chaperone-mediated autophagy (CMA) occurs in lysosomes and selectively degrades unfolded or misfolded protein substrates with KFERQ-like motifs [19]. The process starts when cochaperones, particularly the heat shock cognate protein of 71 kDa (HSC70), recognize the KFERQ-like motif in these protein substrates. Subsequently, other

* Corresponding author.
** Corresponding author.
E-mail addresses: limy2013@sina.com (M. Li), yslal@163.com (S. Yin).

https://doi.org/10.1016/j.cbi.2024.111341
Received 2 September 2024; Received in revised form 15 November 2024; Accepted 3 December 2024
Available online 4 December 2024

cochaperones—including heat shock protein (Hsp) 40, Hsp90, and Bcl-2-associated athanogene 1 protein (Bag-1)—join in to assist HSC70 in forming the translocation complex [20]. During this process, Hsp40 enhances chaperone activity, while Hsp90 identifies flexible regions of the protein substrates to prevent aggregation. Concurrently, Bag-1 disrupts the binding of the substrate to HSC70 and lowers its ATPase activity, which inhibits CMA [21]. The translocation complex is then directed to the lysosome via lysosomal-associated membrane protein type 2A (Lamp2A), leading to the degradation of the substrate with the KFERQ-like motif [22]. Dysfunctional CMA can lead to the aggregation of misfolded proteins in the cytoplasm, triggering apoptosis and compromising cellular physiological function [23]. Numerous studies have suggested that impaired neuronal CMA may contribute to the pathogenesis of various neurological disorders, including neurodegenerative diseases, epilepsy, dementia, and cognitive impairment ([24–26]; Tomoda et al., 2020; [27,28]). However, the role of CMA dysfunction in DFX-induced neurotoxicity and its underlying mechanisms require further elucidation.

This study aimed to clarify the neurotoxicity associated with DFX exposure and to further elucidate its underlying toxicological mechanisms. Mice were subjected to intravenous DFX exposure once every other day for 35 days. Iron levels in the peripheral and central nervous systems were assessed using inductively coupled plasma mass spectrometry (ICP-MS). Behavioral tests were conducted to evaluate the emotional and cognitive functions of the mice, providing further insights into the neurotoxic effects. Additionally, we examined neurotransmitter release, neuronal morphology, and CMA function to better understand the underlying toxicological mechanisms. Furthermore, neuronal PC12 and microglia N9 cells were used to investigate the direct cytotoxic effects of DFX on neuronal cells and to confirm the role of CMA dysfunction in the neurotoxicity associated with DFX exposure *in vitro*. The study findings provide evidence for the comprehensive monitoring and timely mitigation of neurotoxic adverse events caused by DFX exposure and lay the groundwork for developing treatments to prevent and address these adverse events, thereby improving patient quality of life.

2. Materials and methods

2.1. Animals

Forty adult KM mice (20 males and 20 females, 6–8 weeks old, 18–22 g) were obtained from Huafukang Biotechnology (Beijing, China). The mice were raised in a specific pathogen-free environment at 22 °C ± 2 °C with a 12-h light–dark cycle. Five mice were housed in each cage and provided with *ad libitum* access to food and water. All animal protocols were developed in alignment with animal welfare principles and were approved by the Institutional Animal Care and Use Committee of Shenyang Pharmaceutical University (SYPU-IACUC-S2024-110-101).

2.2. Exposure plan

After acclimating for 3 days, the mice were randomized into two groups. The DFX exposure group received intravenous injections (4.0 mg/kg) (NOVARTIS, Switzerland) once every other day for 35 days (total of 17 injections). The control group received intravenous saline injections on the same schedule.

2.3. Anxious/depressive behavior assessment

Behavioral tests were conducted to examine anxiety and depressive states in a dark, quiet room to limit interference. A video tracking system (Xinruan Information Technology, China) was used to record and analyze animal behavior.

2.3.1. Open field test

Anxiety-related behavioral changes were evaluated in an open field test (OFT). The OFT was conducted on DFX exposure days 0, 7, 14, 21, 28, and 35. Briefly, the mice were placed in one corner of the open field (50 × 50 cm). Spontaneous activity, measured as average speed, total distance, and time spent in the central, peripheral, and corner zones of the open field (21 × 21 cm), was recorded over 5 min. Feces and urine left in the open field were cleaned with water to avoid interference caused by odor [29].

2.3.2. Tail suspension test

On the 22nd day of DFX exposure, the tail suspension test (TST) was conducted to measure depressive status. Briefly, the mouse was hung upside down from a metal rod 50 cm above a table. Immobility time, which is the time spent without limb movement, was measured. During the 6-min test, the mice were allowed to adapt for 2 min, and then immobility time within the last 4 min was recorded [30].

2.3.3. Forced swimming test

On the 24th day of DFX exposure, the forced swimming test (FST) was conducted to measure depressive status. Briefly, the mouse was placed in a cylindrical plastic container (30 cm high × 11 cm diameter) filled with 25 cm of water maintained at 24 °C ± 1 °C. The immobility time refers to the time when the mouse does not move any limbs. During the 6-min test, the mice were allowed to adapt for 2 min, and then immobility time during the last 4 min was recorded [31].

2.4. Cognitive behavior assessment

2.4.1. Morris water maze test

On the 25th day of DFX exposure, we used the Morris water maze (MWM) (Xinruan Information Technology) to measure learning ability and spatial memory. The MWM is a circular container, 35 cm high and 120 cm in diameter, with a submerged platform and filled with 20 cm of water maintained at 25 °C ± 2 °C. The MWM test was performed over 6 days in two phases. For the first 5 days, the mouse was guided and trained to land on the submerged platform within 1 min, known as the positioning navigation phase. When the mouse failed to find the platform, it was guided and made to stand on it for 15 s. The escape latency, swimming distance, and swimming trajectories within the 1 min were recorded. We removed the platform for the space exploration experiment on the sixth day. The swimming time, distance, time spent in the target quadrants, and the times that mice crossed the original location of the platform within 1 min were recorded [32].

2.4.2. Novel object recognition test

On the 30th day of DFX exposure, the novel object recognition (NOR) test was conducted to assess short-term memory. The NOR test was performed in a 53-cm square box. On the first 2 days, the mice were placed in the square box for 5 min to acclimate to the environment. On the third day, two identical objects were placed in the box, and the mouse was allowed to explore for 5 min. After 1 h, one of the objects was replaced with a novel object, and the mouse was allowed to explore for another 5 min. Exploration was defined as occurring when the distance between the mouse and the object was <2 cm and the object was touched and smelled. The time the mouse spent exploring the novel object and the familiar object was recorded. The recognition index (RI) was calculated as $\frac{TN}{TN+TF} \times 100\,\%$. The testing box was cleaned with water after each mouse experiment [33].

2.4.3. Y maze test

On the 33rd day of DFX exposure, the Y maze test was conducted to examine spatial memory [32]. The Y maze has three symmetrical arms at 120° angles, designated A, B, and C. Each arm is 20 cm long × 10 cm wide × 20 cm high. Mice were subjected to two trial Y maze tests to

assess their spatial memory. In the first trial, the mouse was placed in the maze for 5 min to adapt to the environment. On the second day, the mouse was placed at the distal end of A and allowed to explore the maze freely for 8 min. Entry times in each arm were recorded, and the percentage of alternations (entry into an arm that differs from the previous two entries) was calculated as $(\frac{Alternations}{Arm\ Entries-2}) \times 100\ \%$. In the second trial, one arm of the Y maze was closed before the mouse was placed into the maze and allowed to explore the other two open arms for 5 min. After 1 h, the closed arm was opened, and the mouse was placed into the maze again to explore all three open arms for 5 min. Times of entry and the time spent in each arm were recorded. The new arm (previously closed arm) entry time/rate was calculated as $\frac{New\ Arm\ Entry\ Time/Rate}{Total\ Entry\ Time/Rate} \times 100\ \%$.

2.5. Iron-related indices

After the behavioral tests, the mice were sacrificed, and the blood was collected in tubes with or without anticoagulant to determine the iron-related indices, including ferritin and hemoglobin. Ferritin and hemoglobin levels were determined using an automated biochemical analyzer and a blood cell analyzer, respectively (Mindray Medical, China).

2.6. Iron levels

Iron levels in the brain and serum were determined by ICP-MS. Briefly, after aspirating the homogenates of brain tissue or serum, 2 mL of nitric acid was added and heated at 150 °C. Once the solutions were clear, the mixtures were heated at 150 °C for another 30 min, then allowed to cool and diluted to 25 mL with water. ICP-MS was performed on a 7500a triple quadrupole ICP-MS QQQ (Agilent, USA) equipped with a microconcentric nebulizer (Meinhard MicroMist, USA), Peltier-cooled double-pass spray chamber, standard torch, and auto-sampler. Data were analyzed using MassHunter workstation version 4.1 (Agilent).

2.7. HPLC–MS/MS determination of monoamine neurotransmitters

Monoamine neurotransmitters dopamine (DA), noradrenaline (NE), and 5-hydroxytryptamine (5-HT) were measured against isoproterenol as the internal standard (IS). Briefly, the mouse brain was dissected and homogenized on ice. Chromatography was performed by gradient elution on an Agilent 1290 system equipped with an Agilent ZORBAX Eclipse Plus-C_{18} column (2.1 × 50 mm, 1.8 μm) at 35 °C. The mobile phase consisted of (A) 0.1 % formic acid in water and (B) acetonitrile at 0.3 mL/min. The injection volume was 5 μL. The gradient elution procedure is shown in Table 1. The mass system with an Agilent 6470 triple quadrupole and electrospray ionization source was used to detect the target analytes and IS. Target compounds were quantified in multiple reaction monitoring mode. Optimized mass ionization parameters are shown in Table 2 [34].

2.8. Histopathology

Neurons were stained with Nissl and fuchsin-aldehyde reagents to observe morphological changes and lipofuscin deposition, respectively.

Table 1
Gradient elution procedure.

Time (min)	A%	B%
0	96	4
1	76	4
2	85	15
4	55	45
6	55	65
7	96	4
8	96	4

Briefly, the brain was fixed with 10 % buffered formalin for 24 h, processed with an automated tissue processor (TKY-TSF, Taikang, China), and embedded in paraffin. The blocks were sectioned (5 μm) on a semiautomatic rotary microtome (Leica, Germany), placed on slides, and dried overnight. The sections were stained using a Nissl (cresyl violet method) (BASO, China) or a lipofuscin staining kit (aldehyde fuchsin method) (DeepMind, China). Observations were made under an optical microscope at 200 × magnification (DS-Ri2, Nikon, Japan).

2.9. Immunofluorescence assay

Fixation, processing, embedding, and slicing procedures for brain slice preparation were performed as described in Section 2.8. The slices were incubated with anti-HSC70 and anti-Lamp2A antibodies (Boster China; Abcam, USA) overnight at 4 °C, then with a secondary antibody (APExBIO, China) for 1 h. The samples were washed with 0.1 M phosphate-buffered saline (PBS) and then sealed with an antifading fixation medium (Beyotime, China). The DAPI-, HSC70-, and Lamp2A-stained neurons in the dentate gyrus (DG) of the hippocampus were observed using a BX40 fluorescence microscope (Olympus, Japan). Images were analyzed using ImageJ software to quantify neurons double-stained with anti-HSC70 and anti-Lamp2A antibodies.

2.10. Transmission electron microscopy

The hippocampus was dissected on ice, then cut into 1 mm^3 pieces and fixed in electron microscopy fixative (Servicebio, China) for 2–4 h. Samples were washed three times with 0.1 M PBS (pH = 7.4), then fixed in 1 % osmic acid in 0.1 M PBS (pH = 7.4) for 2 h and washed three more times with 0.1 M PBS. After dehydration, permeation, and embedding (SPI-CHEM/SPI-PON 812 kit, USA), the tissue was cut into sections using an ultramicrotome (Leica UC7, Germany) and double-stained with a 2 % saturated alcohol solution of uranium acetate and lead citrate for 15 min. Samples were observed by transmission electron microscopy (HITACHI HT7700, Japan).

2.11. Cell culture

Mouse microglia N9 and pheochromocytoma PC12 cell lines were incubated in Dulbecco's Modified Eagle Medium containing 10 % heat-inactivated fetal bovine serum, 1 % penicillin, 1 % streptomycin, and 1 mmol/L L-glutamine. Cells were incubated in culture dishes at 37 °C and 5 % CO_2.

2.12. 3-(4,5-Dimethylthiazol-2-yl)-2,5-diphenyltetrazolium bromide assays

DFX neurotoxicity was measured using the 3-(4,5-dimethylthiazol-2-yl)-2,5-diphenyltetrazolium bromide (MTT) assay [35]. Cells were harvested in the logarithmic growth phase, suspended at 1.5 × 10^5 cells/mL, and then seeded in 96-well plates. After incubation for 24 h, DFX (10, 20, 50, or 100 μmol/L) was added and incubated for 72 h. Subsequently, 10 μL of MTT solution (2.5 mg/mL) was added and incubated for another 3–4 h. The medium was removed, and 100 μL of dimethyl sulfoxide was added to dissolve the violet crystal of formazan in cells. A BioTek Synergy™ HT plate reader was used to measure absorbance at 492 nm.

2.13. Determination of cell apoptosis

We used terminal deoxynucleotidyl transferase–mediated dUTP nick-end labeling (TUNEL) staining to measure apoptosis in the brains of the experimental mice. Sample fixing, processing, embedding, and cutting procedures are described in Section 2.8. TUNEL staining was performed according to the manufacturer's instructions. Annexin V-PI double staining was used to measure apoptosis. The CMA agonist AR7

Table 2
Optimized mass parameters for analytes and ISs.

	Compounds	Precursor Ion	Product Ion	Fragmentor	Collision Energy	Cell Accelerator Voltage	Polarity
1	Noradrenaline	274.2	274.2	50	10	3	Positive
2	Isoproterenol(IS)	212.1	119.1	130	20	5	Positive
3	5-hydroxytryptamine	177	160	43	5	5	Positive
4	Dopamine	154	137	47	5	5	Positive

(MedChemExpress, China) was used to validate the pathogenic role of CMA in DFX-induced apoptosis. Log-phase PC12 cells were adjusted to 2 × 10^5 cells/mL and seeded in six-well plates. After pretreatment with AR7 (2.5 μmol/L) for 24 h, DFX (100 μmol/L) was added and incubated for 48 h before the cells were harvested. According to manufacturer instructions (UELANDY, China), Annexin V-FITC (5 μL) and PI (10 μL) in binding buffer (500 μL) were added and incubated for 15 min at 25 °C. Apoptotic cells were then quantified by flow cytometry and analyzed with FlowJo v10.8.1. The cells were also collected for Western blot analysis of HSC70 and Lamp2A.

2.14. Western blot analysis

The mouse hippocampus was dissected and homogenized manually in a radioimmunoprecipitation assay buffer. Protease and phosphatase inhibitors were added to inhibit protein degradation. Total protein concentration was determined using a BCA assay kit (Beyotime). Proteins were separated by 8 % and 12 % SDS-polyacrylamide gels, transferred to polyvinylidene fluoride membranes (Merck Millipore, USA), blocked in rapid blocking buffer (Boster), and incubated with primary antibodies targeting cleaved caspase-3, cleaved PARP, HSC70, Lamp2A, HSP40, LC3-I, LC3-II, and GAPDH (Boster) for 12 h at 4 °C. The membranes were labeled with secondary antibodies for another 1 h (ANPEXIO, China), incubated with enhanced chemiluminescence reagent (Sigma-Aldrich, USA), and imaged using a gel imaging system (BioRad, USA) [35].

2.15. Data analysis

Results are reported as mean ± standard error. Significant differences were analyzed by an independent sample *t*-test or two-way ANOVA (SPSS 22.0, USA). $*p < 0.05$, $**p < 0.01$, $***p < 0.001$ were considered significant compared to the control.

3. Results

3.1. DFX exposure reduces iron levels in mice

As an iron chelator, we first investigated the effects of DFX exposure on peripheral iron levels in mice by detecting serum iron, ferritin, and hemoglobin levels. Our results demonstrate that the mice exposed to DFX had significantly lower serum iron and ferritin levels than the control mice (Fig. 1A and B). DFX exposure could decrease the hemoglobin level of mice (Fig. 1C). Moreover, DFX exposure could affect the iron level in the central nervous system. The brain iron levels of mice exposed to DFX were significantly lower than those of the control mice (Fig. 1D). Our results indicated that DFX exposure not only significantly decreased the peripheral iron level but also decreased the iron level in the central nervous system.

3.2. DFX exposure induces anxious/depressive behavior in mice

We used OFT, FST, and TST to evaluate anxious/depressive behavior in mice exposed to DFX, the test schedule is shown in Fig. 2A. Our results revealed that anxious behavior increased with time of DFX exposure in the OFT, with significant anxious behavior becoming evident in the fifth week. Compared to the control mice, DFX-exposed mice exhibited shorter movement distances and time in the central zone and shorter total distances in the open field. However, the average velocity of mice did not show significant difference, suggesting that DFX exposure did not affect locomotor ability (Fig. 2B–F). DFX-exposed mice exhibited longer immobility times than the controls in the TST and FST, suggesting that DFX exposure could lead to significant depressive behavior (Fig. 2G and H). In sum, these results indicated significant DFX-related anxious and depressive behavior in mice.

3.3. DFX exposure impairs learning and spatial memory in mice

To assess cognitive function, we conducted the MWM test to evaluate learning ability and spatial memory in mice exposed to DFX. Our results indicated that over the course of the positioning navigation experiment from the first day to the fifth day, the path length and escape latency for control mice and those exposed to DFX decreased progressively. On days 4 and 5 of the MWM test, DFX-exposed mice took significant longer paths and more time to escape than control mice, suggesting that DFX exposure significantly impaired their learning ability (Fig. 3A–C). Fig. 3I illustrates the representative trajectory of the mice in the positioning navigation experiment on the fifth day. In the spatial exploration test on the sixth day, DFX-exposed mice exhibited significantly fewer crossings of the platform, spent less time in the hidden platform quadrants, and covered shorter distances in those quadrants than control mice. This indicates that DFX exposure significantly impaired spatial memory (Fig. 3D–F). Fig. 3J shows the representative trajectory of the mice in the spatial exploration experiment on the sixth day. The average speed and total distance traveled by both groups of mice during the MWM did not reveal any significant differences, suggesting that the physical fitness of

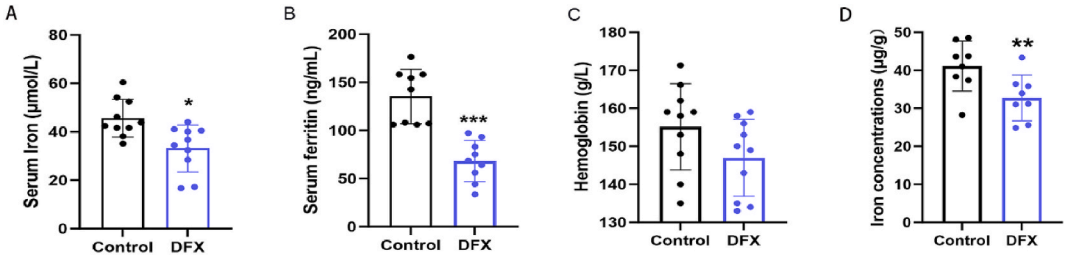

Fig. 1. DFX exposure reduces iron levels in mice. Graphs show (A) iron levels in serum (B) ferritin levels in serum (C) hemoglobin levels (D) iron concentrations in mice brains after DFX exposure for 35 days. Data were shown as Mean ± S.E., n = 8–10 mice/group. The significance differences were compared by using independent *t*-test. $*p < 0.05$, $**p < 0.01$, $***p < 0.001$ vs. Control group.

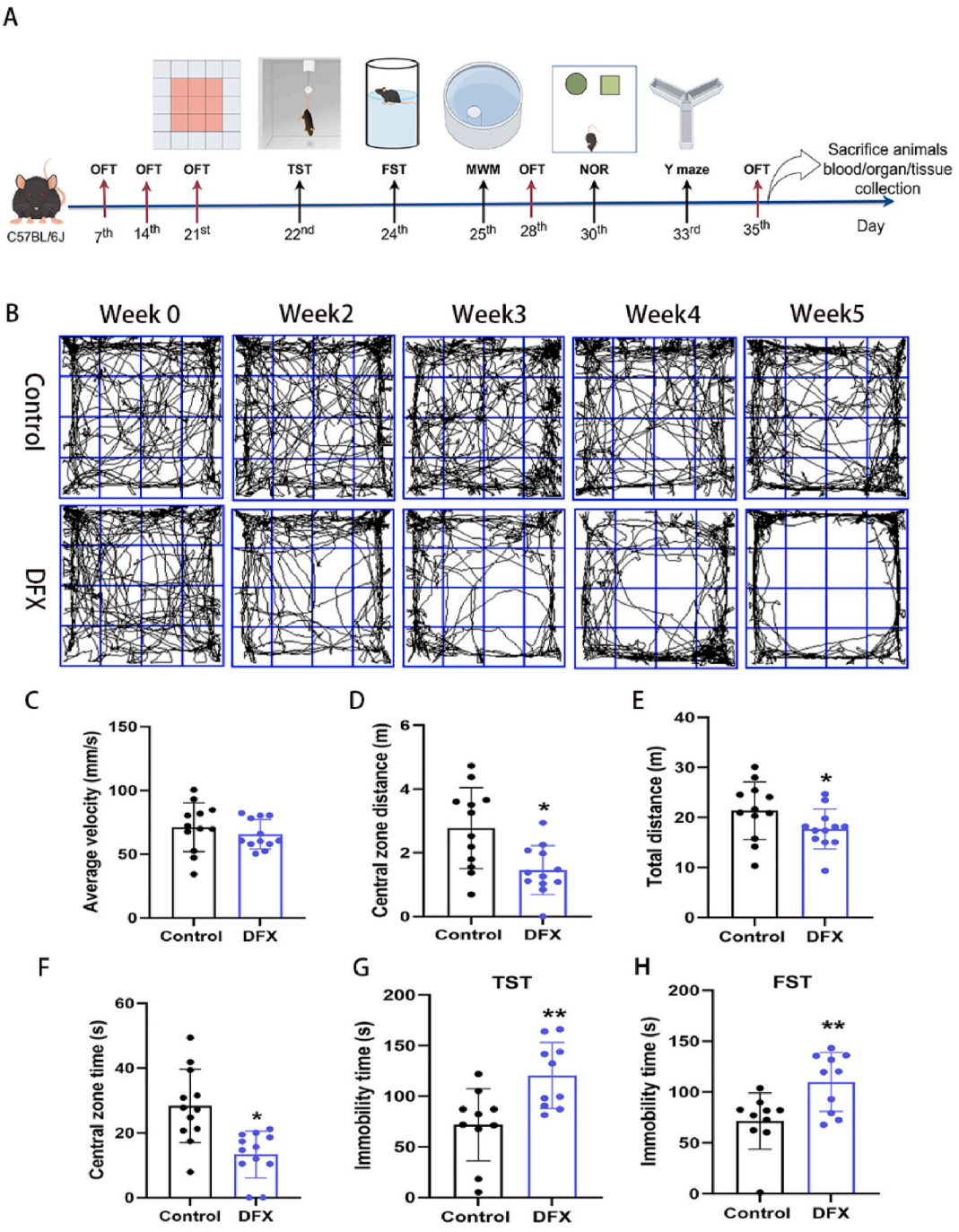

Fig. 2. DFX exposure induces anxious/depressive behavior in mice. Graphs show the (A) workflow of behavioral tests (B) representative trajectory of the control mice and DFX administrated mice from the 1st week to the 5th week, and (C) the average velocity, (D) movement distance in central zone, (E) total movement distance and (F) central zone time in the open field on the 5th week. Graphs also show the immobility time of mice in the (G) TST and (H) FST. Data were shown as Mean ± S.E., n = 10 mice/group. The significant differences were compared by using independent *t*-test. $^{*}p < 0.05$, $^{**}p < 0.01$ vs. Control group.

the mice was not affected by DFX exposure (Fig. 3G and H). Overall, these results suggest that DFX exposure can significantly impair learning ability and spatial memory in mice.

3.4. DFX exposure impairs working memory in mice

We used the Y maze and NOR tests to evaluate the effects of DFX on working memory. In the Y maze, DFX-exposed mice had much poorer spatial recognition memory than control mice. These mice had a lower alternation rate in the spontaneous alternation test (Fig. 3K) and spent less time entering the new arm in the spatial cognition test (Fig. 3L). However, the new arm entry rate did not differ between groups (Fig. 3M). In the NOR test, the DFX-exposed mice showed a significantly lower RI than the control mice (Fig. 3N), suggesting that DFX exposure significantly impaired short-term memory in mice. These results demonstrate that DFX leads to working memory impairment in mice.

3.5. DFX exposure leads to disordered neurotransmitter release in mice

The release of monoamine neurotransmitters is related to the emotional and cognitive functions of the central nervous system [34]. Due to the impairment of neurological functions in mice caused by DFX

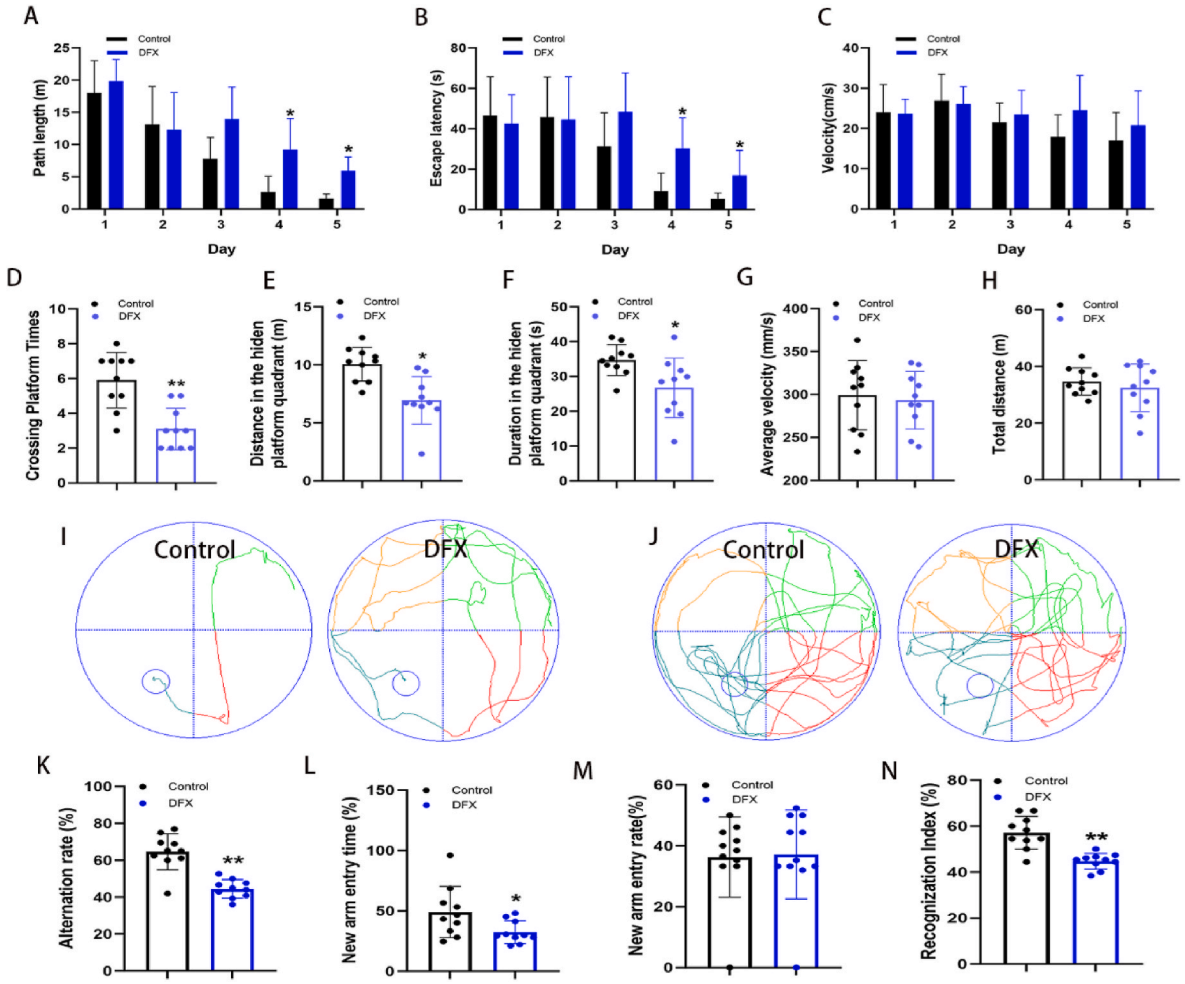

Fig. 3. DFX exposure impairs cognitive function in mice. Graphs show the (A) path length, (B) escape latency and (C) velocity in the positioning navigation experiment. Data were shown as Mean ± S.E., n = 10 mice/group. The significant differences were compared by using two-way ANOVA. *$p < 0.05$ vs. Control group. Graphs show the (D) crossing platform times, (E) distance, (F) duration (G) average velocity and (H) total distance in the hidden platform quadrant in the space exploration experiment. Graphs show the representative (I) trajectory of mice in positioning navigation experiment and (J) trajectory of mice in space exploration experiment in MWM. Graphs show the (K) alternation rate, (L) new arm entry time, (M) new arm entry rate of mice in Y maze and (N) recognition index in NOR test. Data were shown as Mean ± S.E., n = 10 mice/group. The significant differences were compared by using independent *t*-test. *$p < 0.05$, **$p < 0.01$ vs. Control group.

exposure, we investigated the effect of DFX on monoamine neurotransmitter release. In the current study, we observed significantly reduced cerebral concentrations of DA, NE, and 5-HT (Fig. 4A–C), suggesting that the emotional and cognitive dysfunctions associated with DFX exposure might be related to disordered monoamine neurotransmitter release in mice.

3.6. DFX exposure induces apoptosis in the hippocampal neurons of mice

Given that the hippocampus is known to play a crucial role in emotional and cognitive functions, we started our investigation by utilizing Nissl staining to assess the morphological changes in the hippocampal neurons in mice exposed to DFX. Our findings revealed significant neuronal damage in the CA1 region of the hippocampus in DFX-treated mice, characterized by nuclear pyknosis, hyperchromatic nuclei, and even cytolysis (Fig. 4D and E). We then analyzed the protein levels of cleaved cysteinyl aspartate–specific protein-3 (caspase-3) and cleaved poly(ADP-ribose) polymerase (PARP), both of which are key mediators of apoptosis [36]. Results demonstrated that DFX exposure significantly increased the protein expression of cleaved caspase-3 and cleaved PARP in the hippocampal neurons of mice (Fig. 4F–H). Additionally, TUNEL staining results indicated a significant increase in the number of positive cells in the hippocampal CA1 region following DFX treatment (Fig. 4I and J). These findings suggest that the behavioral alterations and neurotransmitter release disorders observed in DFX-exposed mice may be linked to neuronal apoptosis in the CA1 region of the hippocampus.

3.7. DFX exposure induces CMA dysfunction in the hippocampal neurons of mice

CMA dysfunction–induced neuronal apoptosis plays a pathogenic role in various neurological diseases [24]. To explore this further, we first assessed the expression of CMA-related proteins in the hippocampus of mice, specifically HSC70, Lamp2A, and Hsp40. Our findings revealed that DFX exposure significantly reduced the protein levels of HSC70, Lamp2A, and Hsp40 in the hippocampal neurons, while the protein levels of LC3-I and LC3-II, which are associated with macroautophagy, remained unaffected by DFX exposure (Fig. 5A–E). Since DG region of the hippocampus has gained considerable attention as both a form of structural plasticity and as a neural substrate for the pathophysiology of major depression disorder (Sahay et al., 2007), we examined the colocalization of HSC70 and Lamp2A within the neuronal cytoplasm of DG area through immunofluorescence double staining to evaluate the functional state of CMA. Our results demonstrated that compared to the control mice, the DFX-exposed mice exhibited weaker luminescence of

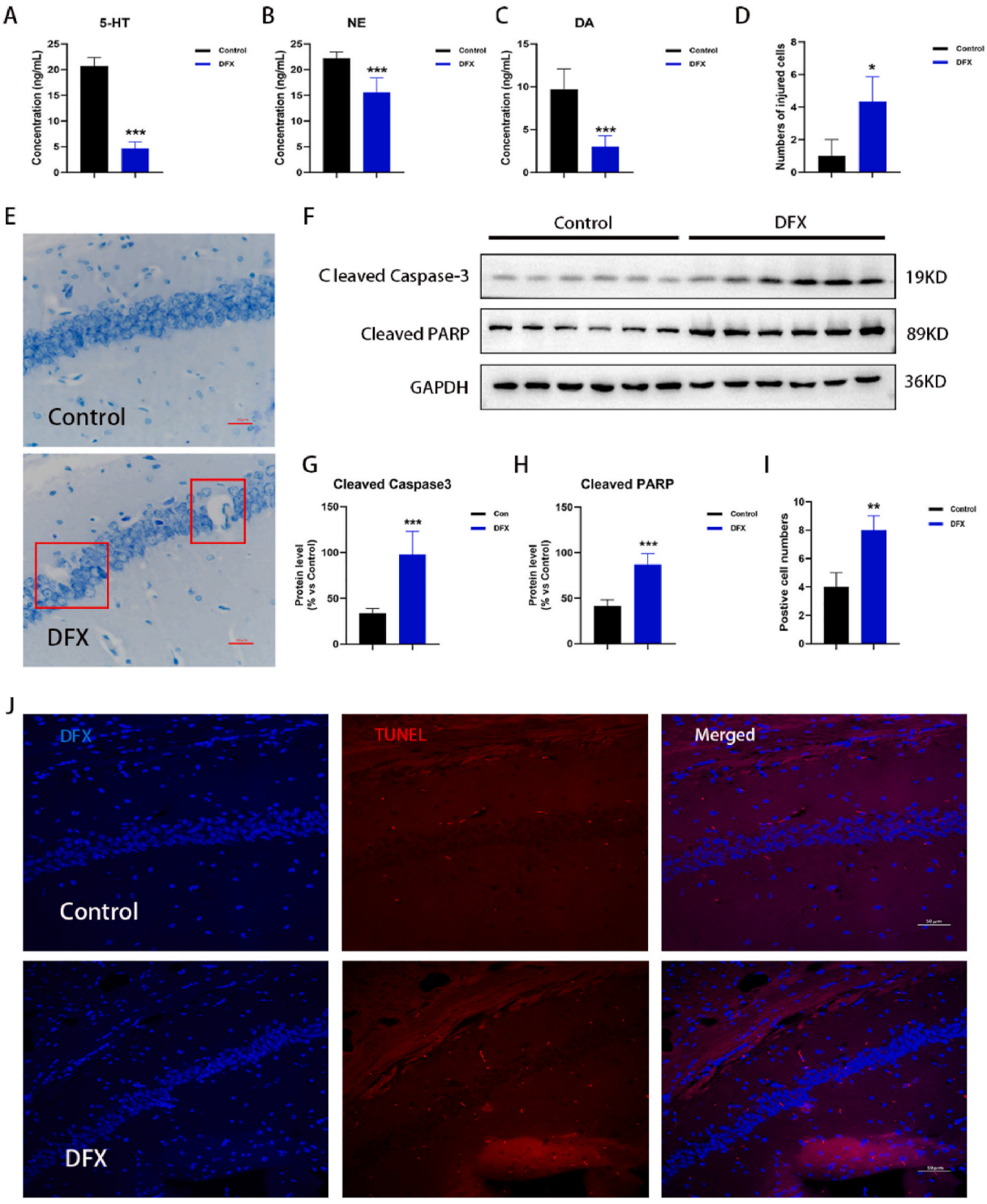

Fig. 4. DFX exposure affects monoamine neurotransmitters release and induces apoptosis in hippocampal neurons of mice. Graphs show the monoamine neurotransmitters that are affected by DFX, including (A) 5-hydroxytryptamine, (B) noradrenaline, (C) dopamine. Graphs show (D) the quantitative statistics of injured cell numbers and (E) representative images of morphological changes in the hippocampal CA1 region, (F) representative images of apoptotic proteins, and protein quantification of (G) cleaved caspase3 and (H) cleaved PARP, and (I) quantitative statistic of positive cell numbers and (J) representative images of TUNEL staining in the hippocampal CA1 region. Scale bar = 50 μm. Data were shown as Mean ± S.E., n = 5 mice/group; n = 3 images/group. The significant differences were compared by using independent *t*-test. $^{*}p < 0.05$; $^{**}p < 0.01$, $^{***}p < 0.001$ vs. Control group.

HSC70 and Lamp2A, along with significantly reduced colocalization of these two proteins in the cytoplasm of the hippocampal neurons in the DG region (Fig. 5F and G). These results suggest that DFX exposure may induce neuronal apoptosis in the hippocampus of mice due to CMA dysfunction.

Lipofuscin is a misfolded protein characterized by a KFERQ-like motif, which makes it recognizable by HSC70 for degradation by CMA. CMA dysfunction can lead to lipofuscin deposition in cells [26]. To determine whether CMA dysfunction was the underlying mechanism of DFX-induced neuronal apoptosis, fuchsin-aldehyde staining was used to

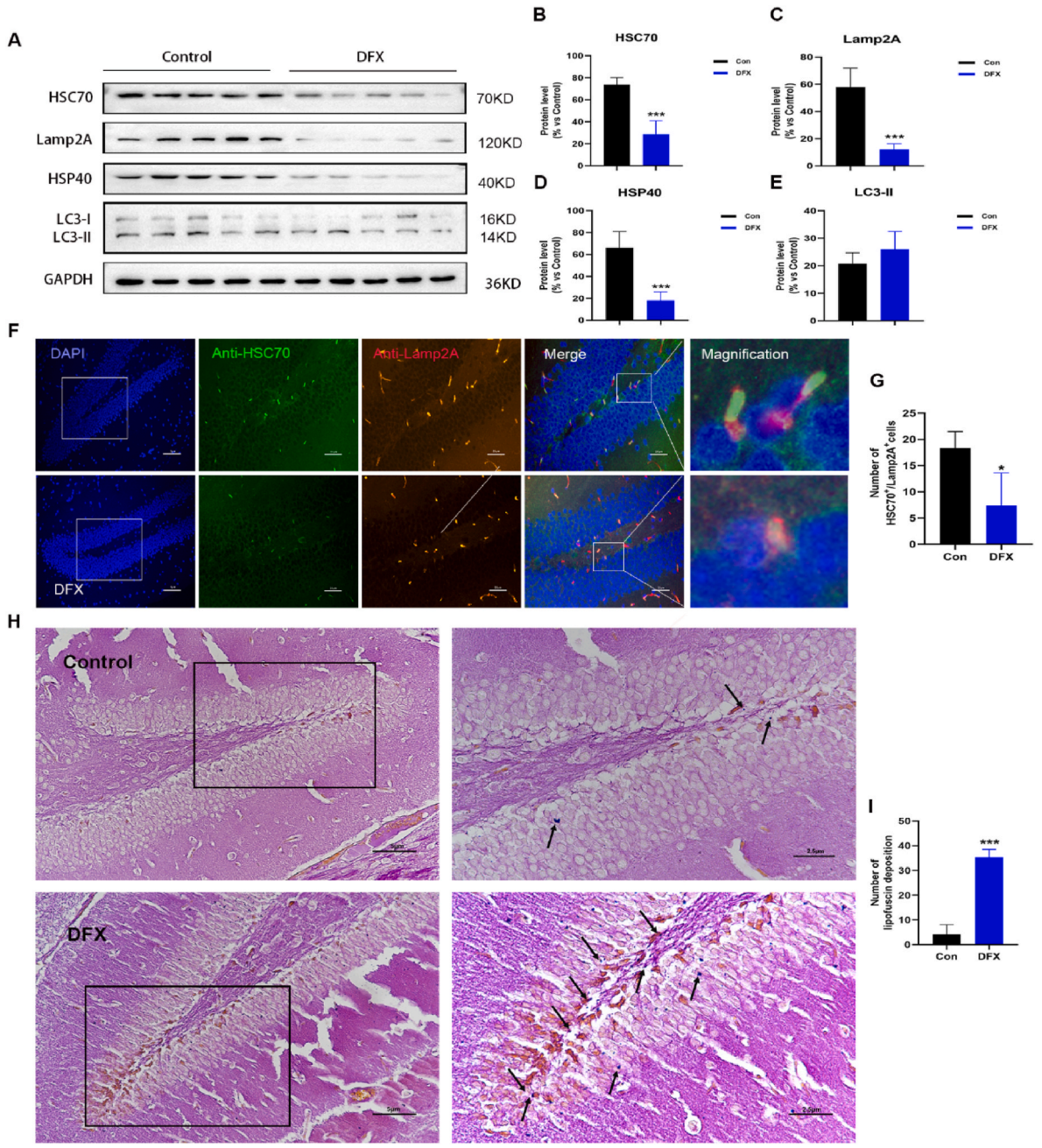

Fig. 5. DFX exposure induces CMA dysfunction in hippocampal neurons of mice. Graphs exhibit the (A) representative protein bands of CMA related proteins, and protein quantification of (B) HSC70, (C) Lamp2A, (D) Hsp40, (E) LC3-II, (n = 5 mice/group). Data were shown as Mean ± S.E., n = 5 mice/group. Graphs show representative immunofluorescence images (F) and quantitative statistics results (G) of the colocalization of HSC70 (green) and Lamp2A (red) in DG region of the hippocampus. Scale bar = 25 or 50 μm. Graphs show (H) the representative fuchsin-aldehyde staining images of DG region of the mice, and the quantitative analysis of fuchsin-aldehyde staining lipofuscin was shown in (I). Scale bar = 2.5 μm or 5 μm. Data were shown as Mean ± S.E., n = 3 images/group. The significant differences were compared by using independent *t*-test. $^{*}p < 0.05$, $^{***}p < 0.001$ vs. Control group. (For interpretation of the references to colour in this figure legend, the reader is referred to the Web version of this article.)

assess the lipofuscin levels in the hippocampal neurons. Comparing DFX-exposed mice to the control group revealed a notable increase in lipofuscin deposition within the neurons of the hippocampal DG region (Fig. 5H and I). These findings suggest that DFX exposure may induce neuronal apoptosis in the hippocampus due to impaired CMA function.

3.8. *DFX exposure leads to ultrastructural changes in the hippocampal neurons of mice*

To understand the role of CMA dysfunction in DFX-induced neuronal apoptosis in the hippocampus, we used transmission electron microscopy to examine ultrastructural changes in the neurons (Fig. 6A). Our results indicated lipofuscin in the cytoplasm of neurons from DFX-exposed mice, confirming the fuchsin-aldehyde staining findings (Fig. 6B). In comparison with control mice, DFX-exposed mice had no autophagosomes and fewer autolysosomes in their hippocampal neurons (Fig. 6C and D). Primary lysosomes, newly formed by the Golgi apparatus, contain hydrolases that have not yet started their digestive functions, whereas autolysosomes contain hydrolases and substrates undergoing digestion. This suggests that DFX causes CMA dysfunction

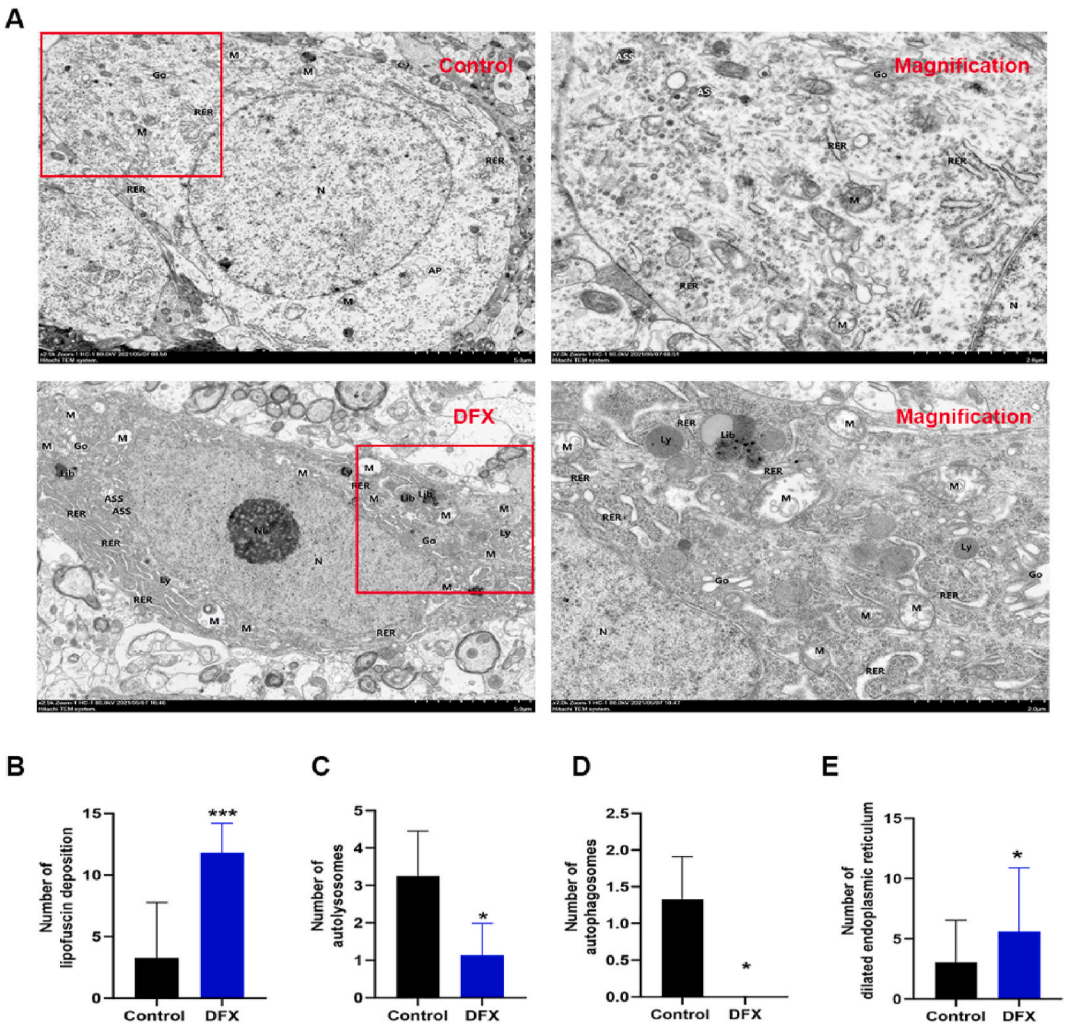

Fig. 6. DFX exposure leads to ultrastructural changes in the hippocampal neurons of mice. Graphs show (A) representative transmission electron microscope images, and quantifications of (B) lipofuscin, (C) autolysosome, (D) autophagosome, and (E) dilated endoplasmic reticulum in hippocampal neurons. Data were shown as Mean ± S.E., n = 3 images for control group and n = 8 images for DFX group. The significant differences were compared by using independent *t*-test. $^{*}p < 0.05$, $^{***}p < 0.001$ vs. Control group. Representative symbols: AP for autophagosome, ASS for autolysosome, Go for golgi apparatus, Lib for lipofuscin, Ly for lysosome, M for mitochondria, N for nucleus, Nu for nucleolus, RER for rough endoplasmic reticulum, SL for secondary lysosome.

and autophagy issues. Additionally, we observed notable dilation of the rough endoplasmic reticulum (Fig. 6E) and other pathological changes, such as cell membrane damage, mitochondrial swelling, and nuclear irregularities in the hippocampal neurons of DFX-exposed mice. Overall, these ultrastructural changes indicate that DFX-induced neuronal apoptosis is linked to CMA dysfunction.

3.9. DFX exposure induces CMA dysfunction and leads to apoptosis in vitro

To determine whether DFX exposure directly impairs neuronal cells, we used the mouse pheochromocytoma cell line PC12 and the mouse microglia cell line N9 to assess neurotoxic effects and examine the mechanism of CMA dysfunction *in vitro*. Our results revealed that DFX exposure caused significant cytotoxicity in the PC12 and N9 cell lines (Fig. 7A and B). Additionally, DFX activated apoptotic-related proteins (Fig. 7C), including increased levels of cleaved caspase-3 and cleaved PARP (Fig. 7D and E). DFX raised the levels of cleaved caspase-9 and Bax, which are linked to mitochondrial apoptosis [36], suggesting that DFX-induced apoptosis may involve mitochondrial activation (Fig. 7F and G). While DFX did not change the levels of LC3-I and LC3-II, it significantly reduced HSC70 and Lamp2A, two CMA-related proteins (Fig. 7H–J). This suggests that DFX exposure leads to CMA dysfunction and apoptosis in neuronal cell lines. To further confirm the role of CMA dysfunction, we used AR7, a specific CMA agonist. Pretreatment of PC12 cells with AR7 significantly reversed DFX-induced apoptosis (Fig. 7K and L) and restored the levels of HSC70 and Lamp2A that DFX had decreased (Fig. 7M – O). Overall, these results support the conclusion that DFX-induced neurotoxicity is linked to neuronal apoptosis due to CMA dysfunction.

4. Discussion

In recent decades, neurological disorders have become the primary cause of disability-adjusted life years worldwide [37], with irreversible neuronal impairment from adverse drug events playing a significant pathogenic role [16,38–41]. Therefore, a thorough evaluation of the neurotoxic effects associated with clinical pharmacotherapy, along with a detailed elucidation of the underlying toxicological mechanisms, is crucial for preventing significant neurological adverse events and mitigating the overall impact on patient health.

DFX is a natural medication used clinically in hematology for treating acute iron intoxication and chronic iron overload [1,2]. Although various neurological adverse events have been reported, such as

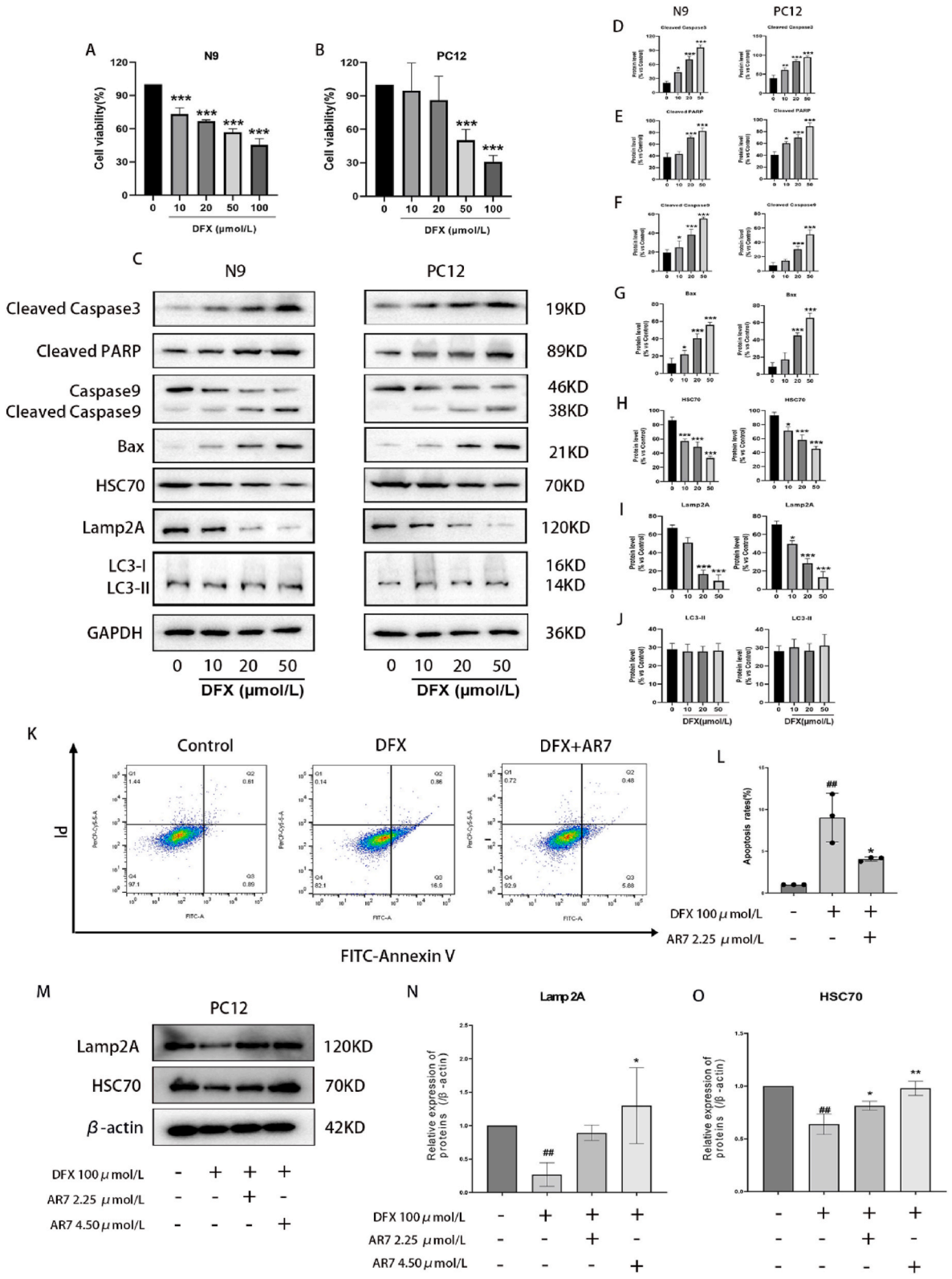

Fig. 7. DFX exposure induces CMA dysfunction and leads to neuronal apoptosis *in vitro*. Graphs show the cell viabilities of (A) N9 cells and (B) PC12 cells, the (C) representative Western blot of apoptotic proteins and CMA related proteins, and protein quantification of (D) cleaved caspase3, (E) cleaved PARP, (F) cleaved caspase 9, (G) Bax, (H) HSC70, (I) Lamp2A, (J) LC3-II. Data were shown as Mean ± S.E., n = 3 independent tests. All statistical comparisons were carried out with an independent *t*-test. $^{*}p < 0.05$, $^{**}p < 0.01$,$^{***}p < 0.001$ vs. Control group. Graphs show (K) representative flowmetry examination of Annexin V-PI double staining, the quantification of apoptosis rates (L), the representative images of Western Blot (M), and the quantitative statistics of Lamp2A(N) and HSC70 (O). Data were shown as Mean ± S.E., n = 3 independent tests. The significant differences were compared by using independent *t*-test. $^{\#\#}p < 0.01$ vs. Control group; $^{*}p < 0.05$; $^{**}p < 0.01$ vs. DFX group.

neuropathies affecting the optical, olfactory, and auditory systems, as well as acute respiratory distress syndrome, these clinical manifestations closely resemble those of iron poisoning, making them challenging to differentiate [17]. Additionally, other severe neurotoxic adverse events, including symptoms such as lethargy, anorexia, transient confusion, and coma, have been documented during the clinical use of DFX [42–44]. Thus, further research is required to clarify whether these neurotoxic adverse events are solely attributable to DFX exposure and to determine the potential impact of DFX on other neurological functions.

In the present study, mice exposed to DFX were able to independently complete the behavioral tests requiring good vision and physical fitness, such as the Y maze, MWM, and NOR test. This indicates that DFX exposure does not cause damage to the optic nerve or severe neurotoxicity such as dizziness, convulsions, or coma, suggesting that these severe adverse events during DFX therapy might not be related to DFX exposure but rather to iron poisoning.

The behavioral tests showed that long-term DFX exposure could lead to significant anxious and depressive behaviors and impaired learning, short-term memory, and working memory in mice. This suggests that DFX exposure could lead to emotional and cognitive dysfunction in mice. Although we found that DFX-exposed mice had lower hemoglobin levels, which can cause fatigue and may affect the results of behavioral tests, there was no significant difference in swimming velocity in the MWM and average velocity in the OFT. These results indicated that the DFX-induced decrease in hemoglobin did not result in significant differences in physical fitness between the control and treatment groups. The depressive behaviors and decreased cognitive function were not related to fatigue but rather to the neurological disorders caused by DFX.

In the current study, DFX exposure significantly decreased iron levels in the peripheral and central nervous systems. Since iron deficiency directly causes neurological dysfunction [45–47], our study suggests that DFX-induced neurotoxicity might be related to iron chelation–induced neuronal iron deficiency, leading to CMA dysfunction and neuronal apoptosis in the hippocampus. While there is currently no literature addressing whether DFX exposure in patients with iron toxicity and chronic iron overload can lead to iron deficiency, our findings suggest that dynamic monitoring of the iron levels of patients during DFX treatment is essential. This vigilance helps prevent iron deficiency resulting from excessive DFX use and protects the nervous systems of patients. Additionally, given the heightened risk of suicide linked to depression, it is critical to assess the mental health status and cognitive function of patients undergoing DFX treatment. Our findings highlight the necessity of establishing a more realistic mouse model of iron overload for future investigations into the long-term toxicity of DFX.

The mechanisms underlying DFX-induced neurotoxicity have been associated with disturbances in other essential transition elements resulting from iron chelation (Deravi, 2014). DFX not only chelates iron ions but also promotes the excretion of zinc and copper [48]. Since the proper functioning of the outer retina and the retinal pigment epithelium relies on adequate concentrations of essential trace elements, particularly copper, the mechanisms of optic neuropathy linked to DFX may be related to deficiencies in zinc and copper (Deravi, 2014; [49]). Additionally, elevated levels of aluminum in cerebrospinal fluid from DFX exposure have been suggested to contribute to the observed neurological deterioration (Ellenberg, 1990; [18]). However, it remains unclear whether DFX exposure can directly impair neurons, and the specific underlying toxicological mechanisms of neurotoxicity require further investigation. This study explored the *in vitro* cytotoxic effects of DFX on neuronal PC12 cells and microglia N9 cells, revealing that the iron-chelating properties of DFX could directly harm neuronal cells. The underlying toxicological mechanism of DFX was found to be CMA dysfunction–associated neuronal apoptosis in the hippocampus. The reversible nature of apoptosis and the recovery of CMA-related proteins by pretreatment with AR7 confirmed this result.

5. Conclusions

Our findings provide compelling evidence that DFX exposure can directly impair neuronal function and lead to significant emotional and cognitive dysfunction in mice. The dysfunction of CMA-induced neuronal apoptosis in the hippocampus plays a pathogenic role in the emotional and cognitive impairments associated with DFX exposure. This study not only emphasizes the importance of regularly monitoring iron levels, as well as the mental health and cognitive function of patients, to prevent severe, irreversible neuropathy from DFX exposure, but also elucidates the underlying toxicological mechanisms of neurotoxicity. This understanding could pave the way for developing treatments aimed at alleviating severe neurological adverse events, ultimately improving the quality of life for patients.

CRediT authorship contribution statement

Hong Zhang: Writing – original draft, Methodology, Investigation, Funding acquisition, Conceptualization. **Jian Guo:** Visualization, Investigation. **Jiayi Chu:** Visualization, Investigation. **Huanhuan Yu:** Visualization, Investigation. **Jialin Zhang:** Visualization, Investigation. **Siman Ma:** Methodology, Investigation. **Ge Jin:** Methodology, Conceptualization. **Yingshan Jiang:** Visualization, Investigation. **Jiao Xiao:** Supervision, Funding acquisition. **Yutong Hou:** Supervision. **Minyan Li:** Writing – review & editing, Supervision, Conceptualization. **Shiliang Yin:** Writing – review & editing, Supervision, Conceptualization.

Funding

This work was financially supported by the National Natural Science Foundation of China (82003971, 82104061), China Postdoctoral Science Foundation (2021M692227), Basic Research Projects of Liaoning Provincial Department of Education (LJKMZ20221364), Doctoral Scientific Research Foundation of Liaoning Province (BS-2022-160), Youth Career Development Plan of Shenyang Pharmaceutical University (ZQN202302).

Declaration of competing interest

The authors declare that they have no known competing financial interests or personal relationships that could have appeared to influence the work reported in this paper.

Acknowledgement

The authors want to thank Professor Yonghong Liu for rendering much assistance in the accomplishment of this research.

List of abbreviations

Bag-1	Bcl-2-associated athanogene 1 protein
Caspase3	cleaved cysteinyl aspartate specific protein-3
CMA	chaperon mediated autophagy
DA	dopamine
DFX	Deferoxamine mesylate
DG	dentate gyrus
DMSO	dimethylsulfoxide
ECL,	enhance chemiluminescence
ESI	electrospray ionization
FST	forced swimming test
HSP	heat shock protein
Hsc70	heat shock cognate protein of 71 KDa
ICP-MS	inductively coupled plasma mass spectrometry
IS	internal standard
Lamp2A	lysosome associated membrane protein 2A

LC3	microtubule-associated protein 1 light chain 3
MTT	3-(4,5-Dimethylthiazol-2-yl)-2,5-diphenyltetrazolium bromide
MWM	*Morris* water maze
NE	noradrenaline
NOR	*Novel object recognition test*
OFT	open field test
PARP	poly ADP-ribose polymerase
RI	recognition index
Tn	total exploration time of novel object
Tf	total exploration time of familiar object
TUNEL,	terminal deoxynucleotidyl transferase dUTP nick end labeling
TST	tail suspension test
5-HT	5-hydroxytryptamine

Data availability

Data will be made available on request.

References

[1] N. Deravi, N. Norouzkhani, K. Keylani, et al., Deferoxamine and other iron chelators. Encyclopedia of Toxicology, fourth ed., 2024, pp. 519–531, https://doi.org/10.1016/B978-0-12-824315-2.00591-1.

[2] M.B. Gary, Iron-chelating therapy for transfusional iron overload, N. Engl. J. Med. 364 (2011) 146–156, https://doi.org/10.1056/NEJMct1004810.

[3] J.L. Kwiatkowski, M. Hamdy, A. Ei-Beshlawy, et al., Deferiprone vs deferoxamine for transfusional iron overload in SCD and other anemias: a randomized, open-label noninferiority study, Blood adv 6 (2022) 1243–1254, https://doi.org/10.1182/bloodadvances.2021004938.

[4] B.A. Davis, J.B. Porter, Long-term outcome of continuous 24-hour deferoxamine infusion via indwelling intravenous catheters in high-risk β-thalassemia, Blood 95 (2000) 1229–1236, https://doi.org/10.1182/blood.V95.4.1229.004k32_1229_1236.

[5] M. Tian, X. Chen, Z.P. Gu, et al., Synthesis and evaluation of oxidation-responsive alginate-deferoxamine conjugates with increased stability and low toxicity, Carbohyd Polym 144 (2016) 522–530, https://doi.org/10.1016/j.carbpol.2016.03.014.

[6] I.Y.R. Adamson, A. Sienko, M. Tenenbein, Pulmonary toxicity of deferoxamine in iron-poisoned mice, Toxicol. Appl. Pharmacol. 120 (1993) 13–19, https://doi.org/10.1006/taap.1993.1081.

[7] M.S. Elalfy, I.A. Abdin, U.R. Ei Safy, et al., Cardiac events and cardiac T2* in Egyptian children and young adults with b-thalassemia major taking deferoxamine, Hematol/Oncol Stem Cell Ther. 3 (2010) 174–178, https://doi.org/10.5144/1658-3876.2010.174.

[8] C. Fabrizio, G. Hickey, R. Ramani, Deferoxamine as a treatment for cardiac siderosis induced cardiomyopathy post liver transplantation, J Heart Lung Trans Pl 40 (2021) S489–S490, https://doi.org/10.1016/J.HEALUN.2021.01.2007.

[9] A. Ponnampalam, D.S. Houston, Acute kidney injury in patients receiving subcutaneous deferoxamine therapy, Blood 121 (2008) 3851, https://doi.org/10.1182/blood.V112.11.3851.3851.

[10] N.B. Bilen, B.P. Gultekin, S. Dagdas, et al., Deferoxamine-related bilateral maculopathy with optical coherence tomography findings, Photodiagn and Photodyn 45 (2024) 103961, https://doi.org/10.1016/j.pdpdt.2023.103961.

[11] P.J. Kertes, T.K.M. Lee, S.G. Coupland, The utility of multif ocal electroretinography in monitoring drug toxicity: deferoxamine retinopathy, Can. J. Ophthalmol. 39 (2004) 656–661, https://doi.org/10.1016/S0008-4182(04)80031-0.

[12] V. Lakhanpal, S.S. Schocket, R. Jiji, Deferoxamine (Desferal®)- induced toxic retinal pigmentary degeneration and presumed optic neuropathy, Ophthalmology 91 (1984) 443–451, https://doi.org/10.1016/S0161-6420(84)34267-1.

[13] R. Haimovici, D.J. D'Amico, E.S. Gragoudas, et al., The expanded clinical spectrum of deferoxamine retinopathy, Ophthalmology 109 (2002) 164–171, https://doi.org/10.1016/S0161-6420(01)00947-2.

[14] E. Delehaye, S. Capobianco, I. Bertetto, et al., Distortion-product otoacoustic emission: early detection in deferoxamine induced ototoxicity, Auris Nasus Larynx 35 (2008) 198–202, https://doi.org/10.1016/j.anl.2007.05.001.

[15] S. Derin, S. Erdogan, M. Sahan, et al., Olfactory dysfunction in β thalassemia major patients treated with iron-chelating agents, Ear Nose Throat J. 98 (2019) 125–130, https://doi.org/10.1177/0145561319840079.

[16] Y. Bentur, M. McGuigan, G. Koren, Deferoxamine (Desferrioxamine) new toxicities for an old drug, Drug Saf. 6 (1991) 37–46, https://doi.org/10.2165/00002018-199106010-00004.

[17] D.W. Christensen, R. Kisling, J. Thompson, et al., Deferoxamine toxicity in hepatoma and primary rat cortical brain cultures, Hum. Exp. Toxicol. 20 (2001) 365–372, https://doi.org/10.1191/096032701680350532.

[18] G.M. Sreenivasan, R.L.M. Yong, D. Holmes, Chronic aluminum toxicity due to intravenous substance abuse managed with deferoxamine chelation therapy: case report, Blood 104 (2004) 3695, https://doi.org/10.1182/blood.V104.11.3695.3695.

[19] O.R. Brekk, M. Markridakis, M. Panagiota, et al., Impairment of chaperone-mediated autophagy affects neuronal homeostasis through altered expression of DJ-1 and CRMP-2 proteins, Mol. Cell. Neurosci. 95 (2019) 1–12, https://doi.org/10.1016/j.mcn.2018.12.006.

[20] N.L. Wankhede, M.B. Kale, A.B. Upaganlawar, et al., Involvement of molecular chaperone in protein-misfolding brain diseases, Biomed. Pharmacother. 147 (2022) 112647, https://doi.org/10.1016/j.biopha.2022.112647.

[21] F.A. Agarraberes, J.F. Dice, A molecular chaperone complex at the lysosomal membrane is required for protein translocation, J. Cell Sci. 114 (2011) 2491–2499, https://doi.org/10.1080/15216540252774810.

[22] S.J. Orenstein, A.M. Cuervo, Chaperone-mediated autophagy: molecular mechanisms and physiological relevance, Semin. Cell Dev. Biol. 21 (2010) 719–726, https://doi.org/10.1016/j.semcdb.2010.02.005.

[23] J.Q. Peng, S.M. Han, Z.H. Chen, et al., Chaperone-mediated autophagy regulates apoptosis and the proliferation of colon carcinoma cells, Biochem Bioph Res Co 522 (2019) 348–354, https://doi.org/10.1016/j.bbrc.2019.11.081.

[24] Y. Li, Z.M. Fan, Q. Jia, et al., Chaperone-mediated autophagy (CMA) alleviates cognitive impairment by reducing neuronal death in sepsis-associated encephalopathy (SAE), Exp. Neurol. 365 (2023) 114417, https://doi.org/10.1016/j.expneurol.2023.114417.

[25] S.P. Panda, Y. Dhurandhar, M. Agrawal, The interplay of epilepsy with impaired mitophagy and autophagy linked dementia (MAD): a review of therapeutic approaches, Mitochondrion 66 (2022) 27–37, https://doi.org/10.1016/j.mito.2022.07.002.

[26] M. Bourdenx, A. Martin-Segura, A. Scrivo, et al., Chaperone-mediated autophagy prevents collapse of the neuronal metastable proteome, Cell 184 (2021) 2696–2714, https://doi.org/10.1016/j.cell.2021.03.048.

[27] Y.F. Zhou, M.Z. Yan, R. Pan, et al., Radix Polygalae extract exerts antidepressant effects in behavioral despair mice and chronic restraint stress-induced rats probably by promoting autophagy and inhibiting neuroinflammation, J. Ethnopharmacol. 265 (2021) 113317, https://doi.org/10.1016/j.jep.2020.113317.

[28] M.M. Tang, T. Liu, P. Jiang, et al., The interaction between autophagy and neuroinflammation in major depressive disorder: from pathophysiology to therapeutic implications, Pharmacol. Res. 168 (2021) 105586, https://doi.org/10.1016/j.phrs.2021.105586.

[29] D.J. Christoffel, S.A. Golden, M. Heshmati, et al., Effects of inhibitor of kappaB kinase activity in the nucleus accumbens on emotional behavior, Neuropsychopharmacology 37 (2012) 2615–2623, https://doi.org/10.1038/npp.2012.121.

[30] L. Steru, R. Chermat, B. Thierry, et al., The tail suspension test: a new method for screening antidepressants in mice, Psychopharmacology 85 (1985) 367–370, https://doi.org/10.1007/BF00428203.

[31] R.D. Porsolt, G. Anton, N. Blavet, et al., Behavioural despair in rats: a new model sensitive to antidepressant treatments, Eur. J. Pharmacol. 47 (1978) 379–391, https://doi.org/10.1016/0014-2999(78)90118-8.

[32] R. Balakrishnan, J.Y. Par, D.Y. Cho, et al., AD−1 small molecule improves learning and memory function in scopolamine-induced amnesic mice model through regulation of CREB/BDNF and NF-κB/MAPK signaling pathway, Antioxidants 12 (2023) 648, https://doi.org/10.3390/antiox12030648.

[33] Q.Q. Huang, C. Zhang, S.H. Qu, et al., Chinese herbal extracts exert neuroprotective effect in Alzheimer's Disease mouse through the dopaminergic synapse/apoptosis signaling pathway, Front. Pharmacol. 13 (2022) 817213, https://doi.org/10.3389/fphar.2022.817213.

[34] H.R. Xu, Z.R. Wang, L. Zhu, et al., Targeted neurotransmitters profiling identifies metabolic signatures in rat brain by LC-MS/MS: application in insomnia, depression and Alzheimer's disease, Molecules 23 (2018) 2375, https://doi.org/10.3390/molecules23092375.

[35] S.L. Yin, R. Wang, F. Zhou, et al., Bcl-xL is a dominant anti-apoptotic protein that inhibits homoharringtonine-induced apoptosis in leukemia cells, Mol. Pharmacol. 79 (2011) 1072–1083, https://doi.org/10.1124/mol.110.068528.

[36] H. Zhang, S.L. Yin, L.H. Wang, et al., Seed oil of Brucea javanica induces apoptosis through the PI3K/Akt signaling pathway in Jurkat acute lymphocytic leukemia cells, Chin. J. Nat. Med. 19 (2021) 608–620, https://doi.org/10.1016/S1875-5364(21)60060-2.

[37] GBD 2021 Nervous System Disorders Collaborators, Global, regional, and national burden of disorders affecting the nervous system, 1990-2021: a systematic analysis for the Global Burden of Disease Study 2021, Lancet Neurol. 23 (4) (2024) 344–381, https://doi.org/10.1016/S1474-4422(24)00038-3.

[38] A. Feola, P. Ciamarra, A. Cavezza, et al., Choking in patients with neurological disorders and role of drug-induced dysphagia, Leg. Med. 69 (2024) 102339, https://doi.org/10.1016/j.legalmed.2023.102339.

[39] M.A. Andersen, R. Gregersen, T.S. Petersen, et al., Association between first-time neurologic events and metronidazole treatment: a case-time control study, Clin. Therapeut. 46 (2024) 307–312, https://doi.org/10.1016/j.clinthera.2024.02.003.

[40] C.Z. Zhou, S.K. Peng, A.Q. Lin, et al., Psychiatric disorders associated with immune checkpoint inhibitors: a pharmacovigilance analysis of the FDA Adverse Event Reporting System (FAERS) database, eClinicalMedicine 59 (2023) 101967, https://doi.org/10.1016/j.eclinm.2023.101967.

[41] M. Jeghers, K. McBennett, E. Roesch, et al., 439 Neurologic and mental health adverse events with CFTR modulator therapies at a cystic fibrosis center, J. Cyst. Fibros. 22 (2023) S230–S231, https://doi.org/10.1016/S1569-1993(23)01365-6.

[42] H. Pall, D.R. Bloke, P. Winyard, et al., Ocular toxicity of desferrioxamine - an example of copper promoted auto-oxidative damage? Brit J Ophthalmol 73 (1989) 42–47, https://doi.org/10.1136/bjo.73.1.42.

[43] M. Rubinstein, P. Dupont, J.-P. Doppee, et al., Ocular toxicity of desferrioxamine, Lancet I (1985) 817–818, https://doi.org/10.1016/S0140-6736(85)91473-4.
[44] D.R. Blake, P. Winyard, J. Lunec, et al., Cerebral and ocular toxicity induced by desferrioxamine, Q. J. Med. 56 (1985) 345–355, https://doi.org/10.1016/0091-7435(85)90085-4.
[45] J.L. Beard, J.R. Connor, Iron status and neural functioning, Annu. Rev. Nutr. 23 (2003) 41–58, https://doi.org/10.1146/annurev.nutr.23.020102.075739.
[46] A. Wassef, Q.D. Nguyen, M. St-Andre, et al., Anemia and Depletion of Iron Stores as Risk Factors for Postpartum Depression: a Literature Review, vols. 1–10, J Psychosom Obst & Gyn, 2018, https://doi.org/10.1080/0167482X.2018.1427725.
[47] H. Zhang, L. He, S.F. Li, et al., Cerebral iron deficiency may induce depression through downregulation of the hippocampal glucocorticoid-glucocorticoid receptor signaling pathway, J. Affect. Disord. 332 (2023) 125–135, https://doi.org/10.1016/j.jad.2023.03.085.
[48] FDA, Desferal (deferoxamine mesylate) for injection. https://www.accessdata.fda.gov, 2007.
[49] S. DeVirgiliis, M. Congia, M.P. Turco, et al., Depletion of trace elements and acute ocular toxicity induced by desferrioxamine in patients with thalassemia, Arch. Dis. Child. 63 (1988) 250–255, https://doi.org/10.1136/adc.63.3.250.